http://dx.doi.org/10.5935/0103-5053.20150314

J. Braz. Chem. Soc., Vol. 26, No. 12, 2629-2639, 2015.
Printed in Brazil - ©2015 Sociedade Brasileira de Química
0103 - 5053 $6.00+0.00

Article

Low Temperature Synthesis of Luminescent $RE_2O_3:Eu^{3+}$ Nanomaterials Using Trimellitic Acid Precursors

Ivan G. N. Silva,[a] Danilo Mustafa,[b] Maria C. F. C. Felinto,[c] Wagner M. Faustino,[d] Ercules E. S. Teotonio,[d] Oscar L. Malta[e] and Hermi F. Brito[,a]*

[a]*Departamento de Química Fundamental, Instituto de Química da Universidade de São Paulo, Av. Prof. Lineu Prestes 748, 05508-900 São Paulo-SP, Brazil*

[b]*Departamento de Física dos Materiais e Mecânica, Instituto de Física da Universidade de São Paulo, Rua do Matão Travessa R 187, 05508-090 São Paulo-SP, Brazil*

[c]*Centro de Química do Meio Ambiente, Instituto de Pesquisas Energéticas e Nucleares, Av. Prof. Lineu Prestes 2242, SP, 05508-000 São Paulo-SP, Brazil*

[d]*Departamento de Química, Universidade Federal da Paraíba, 58051-900 João Pessoa-PB, Brazil*

[e]*Departamento de Química Fundamental, Universidade Federal de Pernambuco, Av. Prof. Moraes Rego, 1235, 50670-90 Recife-PE, Brazil*

[RE(TLA)·$(H_2O)_n$:Eu^{3+}] (RE^{3+}: Y, Gd and Lu; TLA: trimellitic acid) precursor complexes were synthesized by an one step aqueous co-precipitation method. After annealing for 1 h, $RE_2O_3:Eu^{3+}$ nanophosphors were formed through the benzenetricarboxylate low temperature thermolysis method (500-1000 °C). The compounds were characterized by using different techniques [elemental analysis (CHN), Fourier transform infrared spectroscopy (FTIR), thermogravimetry (TG/DTG), X-ray powder diffraction (XPD) and scanning electron microscope (SEM)]. The XPD data indicated that the $Y_2O_3:Eu^{3+}$ materials have crystallite size range from 11 to 62 nm. The SEM and transmission electron microscopy (TEM) images show that the annealed materials keep morphological similarities with the precursor complexes. The photoluminescence properties were studied based on the excitation and emission spectra, and luminescence decay lifetimes of the $^5D_0$ emitting level of the Eu^{3+} ion. The experimental intensity parameters (Ω_λ), lifetimes (τ), as well as radiative (A_{rad}) and non-radiative (A_{nrad}) decay rates were calculated and discussed. The $RE_2O_3:Eu^{3+}$ phosphors (RE: Y^{3+} and Lu^{3+}) annealed at 500 to 1000 °C have emission quantum efficiency (intrinsic quantum yield) values from 60 to 82%, indicating that this material can be potentially used for optical markers applications.

Keywords: low temperature method, benzenetricarboxylate precursors, rare earth sesquioxides, photoluminescence materials

Introduction

Polycarboxylate ligands have a wide variety of structure providing large range of chemical properties when combined with metal ions. It has been drawing the attention in the areas such as metal framework systems (MOF),[1,2] selective markers for medical applications,[3] magnetic materials,[4] gas storage,[5] drug delivery,[6] precursors for materials,[7] etc.

Rare earth (RE) containing materials show a versatility for application in the areas of science and technology specially in catalysis, permanent magnets in hybrid cars batteries,[8,9] electroluminescent materials, persistent phosphors, structural probes, luminescent markers, display panels, etc.[10-15] Most of those applications are consequence of their intrinsic characteristic: sharp intraconfigurational $4f^N$ transitions, archiving high monochromatic emission colors and a wide range of emissions, from infrared to ultraviolet,[16] e.g., Nd^{3+}, Eu^{3+}, Gd^{3+}, Tb^{3+} and Tm^{3+} ions which emit in the infrared, red, ultraviolet, green and blue regions, respectively.

*e-mail: hefbrito@iq.usp.br

One very important feature of the RE^{3+} is their 4f-4f transitions, forbidden by the Laporte's rule. Associated to that, the shielding from the chemical environment by the filled 5s and 5p sub-shells[17] over the 4f electrons lead to a characteristic sharp lines spectra with small absorptivity and emission intensities. Taking into account the RE^{3+} intraconfigurational transitions, these ions can be divided in four groups depending on their spectroscopic features:

(*i*) $Sc^{3+}(3d^0)$, $Y^{3+}(4d^0)$, La^{3+} $(4f^0)$ and $Lu^{3+}(4f^{14})$ where the 4f electrons are non-optically active due to their completely empty or fully occupied subshells;[16]

(*ii*) $Gd^{3+}(4f^7)$ is a singular case due to its half-filled 4f layer, and therefore very stable. The energy difference between the lower emitting level ($^6P_{7/2}$) and the fundamental level ($^8S_{7/2}$) is approximately 32000 cm^{-1} opening the opportunity for its application as inorganic matrices. Due to the chemical similarity with other RE^{3+} ions, it is extensively used to study the emission of the ligands in coordination complexes;

(*iii*) $Sm^{3+}(4f^5)$, $Eu^{3+}(4f^6)$, Tb^{3+} $(4f^8)$ and $Dy^{3+}(4f^9)$: in these ions, the energy gap between the emitting and the lower levels are large enough to reduce the non-radiative decay process and accept energy from the ligands, interconfigurational transitions or charge transfer bands excited levels (Figure 1);

(*iv*) $Ce^{3+}(4f^1)$, $Pr^{3+}(4f^2)$, Nd^{3+} $(4f^3)$, $Ho^{3+}(4f^{10})$, $Er^{3+}(4f^{11})$, $Tm^{3+}(4f^{12})$ and Yb^{3+} $(4f^{13})$: in these ions the energy gap between the emitting and lower levels are small, increasing the non-radiative decay process usually mediated by high energy vibrational modes in ligands (typically water molecules) or matrices (oxycarbonates, hydroxides, etc.). In these cases, the process accounts for the decreasing in the final emission efficiency.

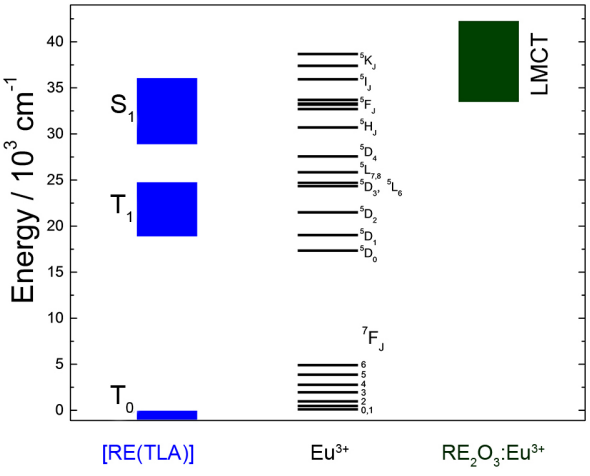

Figure 1. Partial energy diagram of trimellitic acid (TLA) ligand from $[RE(TLA)\cdot(H_2O)_n]$ (RE^{3+}: Y, Gd and Lu) precursor (singlet and triplet states), Eu^{3+} ion and RE_2O_3:Eu^{3+} (LMCT) state.

To overcome the small absorptivity coefficients, luminescence sensitizers can be used to absorb and transfer the energy efficiently to the RE ions, keeping their desirable atomic characteristics. This phenomenon is a key feature in design of luminescent materials.[16,18,19]

In inorganic matrices such as vanadates, molybdates, tungstates and sesquioxides containing RE^{3+} ion, generally is observed an efficient energy transfer from the ligand metal charge transfer (LMCT) band to the metal ions. In the special case, the Eu^{3+} ion shows a high absorption intensity arising from the allowed LMCT transition, yielding a high intensity luminescence.[20]

In solid state reactions, typically, is necessary high temperatures and long reaction time periods to prepare luminescent materials. This way to synthesize materials is known as ceramic method, which promotes heterogeneous distribution of the activator ion within the matrix and generate materials with high crystallite and particle sizes. Alternative methods to obtain materials in milder reaction conditions as: sol-gel, combustion or Pechini methods,[21,22] are key to overcome the experimental limitation and improve their properties.

This report demonstrate the synthesis, characterization and optical properties of [RE(TLA):Eu^{3+} (x mol%)] complexes (RE^{3+}: Y, Gd and Lu; x: 0.1, 0.5, 1.0, and 5.0 mol%) and their low temperature annealing into the high luminescent RE_2O_3:Eu^{3+} phosphors. All the precursor complexes and resulting nanophosphors were characterized by elemental analysis (CHN), Fourier transform infrared (FTIR), thermogravimetry (TG), derivative thermogravimetry (DTG), X-ray powder diffraction (XPD) and scanning electron microscopy (SEM). The photoluminescence properties of the doped materials were studied based on the excitation and emission spectra and luminescence decay curves of the Eu^{3+} ion $^5D_0$ excited level.

Experimental

High purity RE_2O_3 (RE^{3+}: Y, Eu, Gd and Lu; CSTARM, 99.99%, China) were used to prepare the respective $RECl_3.(H_2O)_6$ salts by reaction with concentrated HCl solution until total decomposition (ca. 60-80 °C) of the solid and final pH close to 6. The trimellitic acid (TLA) (in the form of 1,2,4-benzenetricarboxylic acid 1,2-anhydride or 1,3-dihydro-1,3-dioxo-5-isobenzofurancarboxylic acid; Aldrich, 97%, Germany) was solubilized in water by drop-wise addition of 1 mol L^{-1} sodium hydroxide up to pH close to 6.

For the preparation of the [RE(TLA):Eu^{3+}] complexes, 50 mL of $RECl_{3(aq)}$ (0.05 mol L^{-1}) was slowly added to a 200 mL solution of $Na_3(TLA)_{(aq)}$ (0.0125 mol L^{-1}) at 1:1

molar ratio at ca. 100 °C. The reaction mixture was refluxed for 1 h, the precipitate was filtered and washed four times with distilled water, dried and stored at reduced pressure.

The [RE(TLA):Eu^{3+}] complexes obtained are non-hygroscopic, white crystalline powders, stable in air. The RE_2O_3:Eu^{3+} nanophosphors were obtained by annealing the [RE(TLA):Eu^{3+}] complexes at 500, 600, 700, 800, 900 and 1000 °C in a static air atmosphere, resulting in RE_2O_3:Eu^{3+} nanophosphors.

Elemental analyses were performed with a Perkin-Elmer CHN 2400 analyzer. The FTIR were acquired from 400 to 4000 cm^{-1} in KBr pallets form by using a Bomem MB100 FTIR. Thermogravimetry was performed from 30 to 900 °C (heating ramp of 5 °C min^{-1}, synthetic air dynamic atmosphere) in a TA HI-RES TGA 2850 equipment. The XPD patterns were obtained in a Miniflex Rigaku II equipment ($CuK_{\alpha 1}$) from 5 to 70° (2θ). The SEM micrographs were recorded in a JEOL JSM 7401F field emission scanning electron microscope. The transmission electron microscope (TEM) micrographs were recorded in a JEOL USA JEM-2100 LaB_6 transmission electron microscope.

The luminescence study was based on the excitation and emission spectra recorded at room (300 K) and liquid nitrogen (77 K) temperatures. The measurements were performed in a SPEX-Fluorolog 3 instrument with double monochromators in front face mode (22.5°) using a 450 W Xenon lamp as excitation source. Luminescence decay curves were obtained by using a 150 W pulsed lamp and recorded in a SPEX 1934D phosphorimeter.

Results and Discussion

Characterization

A combination of elemental and thermogravimetric analysis (Table S1 and Figure 2) suggests an 1:1 molar ratio between the RE^{3+} ion and TLA ligand ([RE(TLA)·$(H_2O)_n$:Eu^{3+}]; n: 4, 4 and 3 for Y^{3+}, Gd^{3+} and Lu^{3+}, respectively).[23] The TG curves of coordination compounds show a water molecules mass-loss in the temperature interval between 50 and 230 °C. Although the organic moiety decomposition of the complexes presents only one single-step between 450 and 570 °C. In this case, it was used annealing temperature of 500 °C during 1 h, in order to eliminate all the organic part leading to formation of the RE_2O_3:Eu^{3+} luminescent material.

The infrared absorption spectra (Figure S1) present similar spectral profile for the RE^{3+} complexes and Eu^{3+}-doped matrices. The absorption bands between 1300 and 1600 cm^{-1} in the FTIR spectra of [RE(TLA)·$(H_2O)_n$:Eu^{3+}]

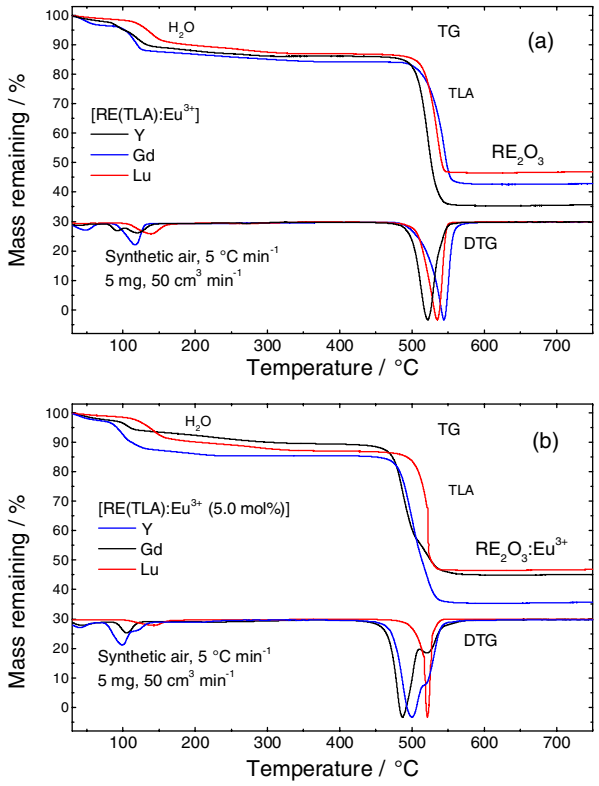

Figure 2. TG and DTG curves (a) [RE(TLA)] and (b) [RE(TLA):Eu^{3+} (5.0 mol%)] (RE^{3+}: Y, Gd and Lu).

are assigned to the carboxylate symmetric ν_s(C=O) and asymmetric ν_{as}(C=O) stretching modes, respectively.[19,24,25] The narrow absorption peak around 3070 cm^{-1} is assigned to the C–H bond stretching of the [RE(TLA):Eu^{3+}] complexes and the broad band between 3100-3700 cm^{-1} correspond to the O–H stretching from the water molecules.[26]

The sharp absorption bands around 510 and 580 cm^{-1} correspond to the characteristic RE^{3+}–O stretching vibration. It is worth mentioning that the broad bands from 1250 to 1600 cm^{-1} are assigned to stretching mode of oxycarbonate remainder from the decomposition of the organic moistly of TLA and decreases with increasing annealing temperature (Figure S1), due to oxycarbonate decomposition.[23] The broad absorption band located from 2800 to 3700 cm^{-1} is assigned to the superficial hydroxyl groups in the nanomaterials. Therefore, the RE_2O_3:Eu^{3+} materials originated from the [RE(TLA)] precursor complexes present similar chemical behavior compared to the sesquioxides prepared from the [RE(TMA)] complexes as reported by Silva *et al.*[23]

The X-ray diffraction patterns of the [RE(TLA):Eu^{3+}] complexes are similar to the powder diffraction patterns (PDF) for [Gd(TLA)]:Eu^{3+} and [Y(TLA)]:Eu^{3+}] (00-056-1733) and [Lu(TLA)]:Eu^{3+}] (00-058-1915), Y^{3+} and Gd^{3+} complexes are isomorphs. Consequently, there is no change in position or formation of new diffraction

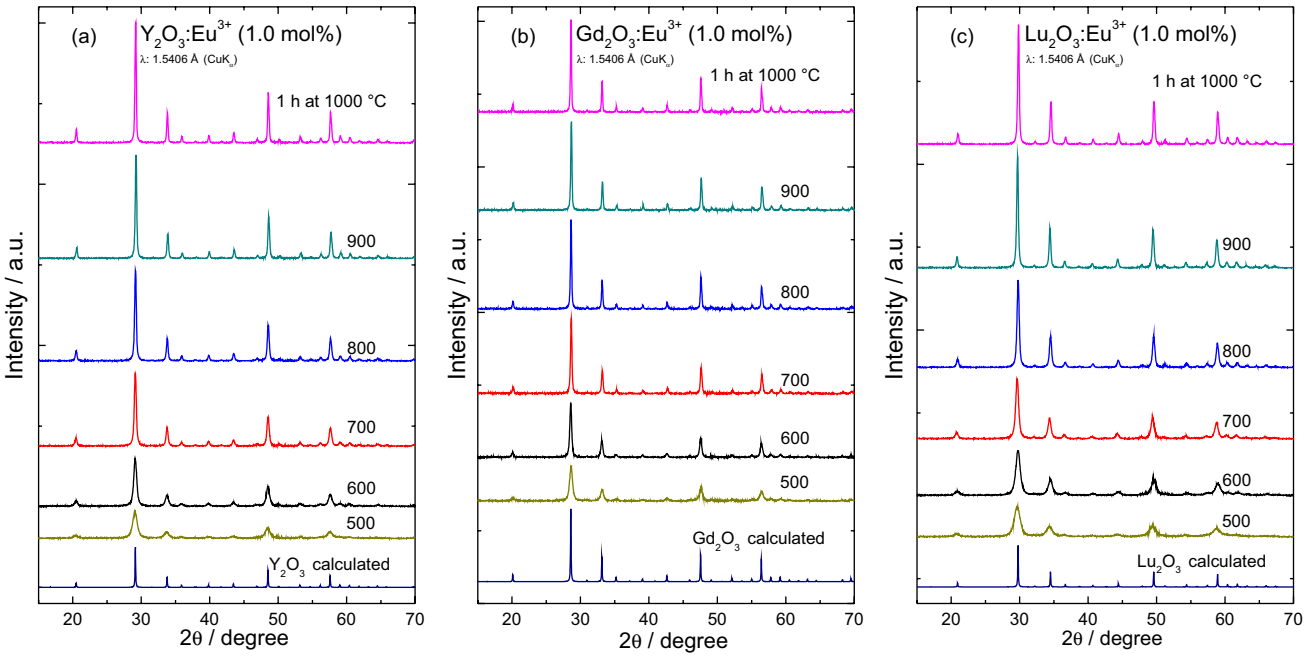

Figure 3. XPD patterns of (a) $Y_2O_3:Eu^{3+}$; (b) $Gd_2O_3:Eu^{3+}$ and (c) $Lu_2O_3:Eu^{3+}$ (1.0 mol%) materials annealed for 1 h at different temperatures; reference pattern: PDF: 86-2477 and 86-2475, respectively.

peaks at different concentrations of the dopants. This result is consistent with the Vegard's rule[27,28] which suggests a formation of a solid solution between the Eu^{3+} dopant and the RE^{3+} in the host matrices due to the high similarity in the radii of these RE^{3+} ions.[27]

The XPD patterns of the annealed materials at 500, 600, 700, 800, 900 and 1000 °C (Figure 3) reveal a formation of $RE_2O_3:Eu^{3+}$ in a cubic phase crystallization with the $Ia\bar{3}$ space group.[29] The absence of 2θ shift and reflections of impurities in the patterns of the $RE_2O_3:Eu^{3+}$ indicates the formation of pure RE^{3+} sesquioxides. The XPD data of the Y_2O_3, Gd_2O_3 and Lu_2O_3 matrices (Figure 3) are very similar. Slight differences in the (222) reflection around 28°, moving to higher 2θ values with decreasing of the ionic radius of the RE^{3+} in the matrix, as predicted by Bragg's law.[30]

The average crystal size of the doped materials was estimated from the powder diffraction data by using the Scherrer's formula (Figure 4).[23,31] The crystallite size of the RE_2O_3 materials increases as function of the RE^{3+} radius and annealing temperature. This behavior can be assigned to the higher reactivity of the Gd_2O_3, with lower melting point (2339 °C) compared to Y_2O_3 (2410 °C) and Lu_2O_3 (2427 °C).[32] Therefore, the sintering process is favored for the gadolinium matrix due to the dependence of the partial melting of the nanocrystals.[23]

The narrowing of the diffraction peaks of $RE_2O_3:Eu^{3+}$ (1.0 mol%) (RE^{3+}: Y, Gd and Lu) phosphors presented in the XPD patterns (Figure 3) as function of the annealing temperature, indicates that the crystallite size increases from 11, 17, 18, 37, 46 and 62 nm as the annealing temperature increases from 500, 600, 700, 800, 900 and 1000 °C (Y_2O_3), respectively (Figure 4). This behavior is related to the sintering of the nanocrystallites favored at high temperatures. Although the $Gd_2O_3:Eu^{3+}$ annealed at 1000 °C was also included in this work, the Scherrer's formula is recommended only for crystallite sizes up to 200 nm (Figure 4).

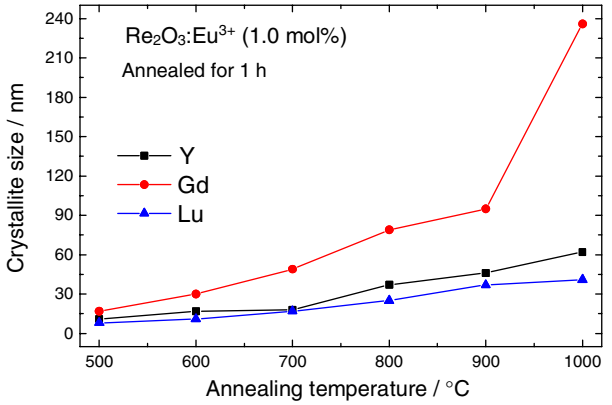

Figure 4. Correlation between the sesquioxides crystallite size and annealing temperature for $RE_2O_3:Eu^{3+}$ (1.0 mol%) materials.

The SEM images of the [RE(TLA):Eu^{3+} (1.0 mol%)] precursors shows rods and a flower like morphologies (stacking of micrometric sheets of the material) for Y^{3+}/Gd^{3+} (Figures 5a and 5b) and Lu^{3+} complexes, respectively (Figure 5c). After annealing up to 1000 °C, the $RE_2O_3:Eu^{3+}$ materials retained the original morphology of the correspond precursor complex (Figures 5d-5f). The nanosesquioxides

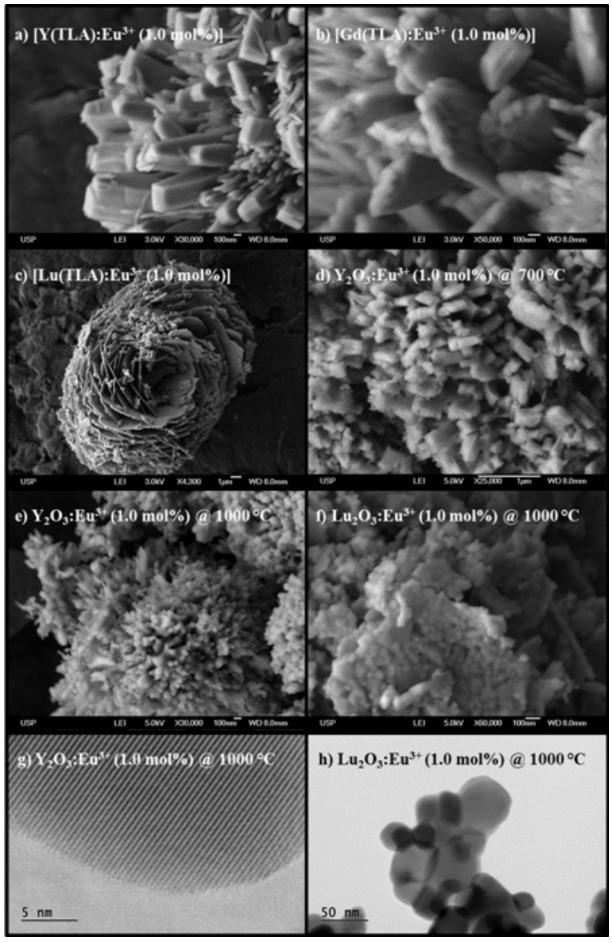

Figure 5. SEM images of [RE(TLA):Eu^{3+} (1.0 mol%)] precursor complexes (a; b; c); RE_2O_3:Eu^{3+} (1.0 mol%) phosphor annealed during 1 h (d; e; f) and TEM images of RE_2O_3:Eu^{3+} (1.0 mol%) annelaed during 1 h at 1000 °C (g; h).

exhibit higher porosity due to the decomposition of the organic moiety. This property is important for the design of nanomaterials with controlled morphology. Since it is possible to modify the complex morphologies, the desired nanoparticle shapes can be obtained by choosing the suitable synthetic method and reaction conditions.[33,34]

The TEM micrographs (Figures 5g and 5h) show the cubic shape of the crystallites with high crystallinity. The particles retained the shape of the precursor agglomerates, shown in the SEM microscopy. At higher magnification no defects were observed in the crystals (except for the edges and crystallite contact points), suggesting the formation of a solid solution between the Eu^{3+} ions and the host matrices, compatible with the similar RE^{3+} ionic radii and chemical behavior of the Eu^{3+} and RE^{3+} matrices.

Photophysical properties of materials

[RE(TLA):Eu^{3+}] precursor complexes

The excitation spectra of [RE(TLA):Eu^{3+} (x mol%)] (RE^{3+}: Y, Gd and Lu) compounds were obtained by monitoring the hypersensitive transition $^5D_0 \rightarrow {}^7F_2$ (619 nm) at 77 K (Figure 6). For all the complexes, the absorption bands are dominated by a high intensity broad TLA ligand band centered at 295 nm assigned to the $S_0 \rightarrow S_1$ transition, indicating an efficient energy transfer TLA $\rightarrow Eu^{3+}$. The sharp peaks are assigned to the absorption of the Eu^{3+} ion originated from the ground state $^7F_0$ to the $^5L_6$ and $^5D_2$ excited levels. The excitation spectra of the [RE(TLA):Eu^{3+} (x mol%)] (RE^{3+}: Y and Gd) compounds show similar profiles suggesting that this system presents equivalent chemical environments around RE^{3+} ions and optical behaviors. On the other hand, [Lu(TLA):Eu^{3+} (x mol%)] shows slightly different spectral profile. For all [RE(TLA):Eu^{3+}] systems, the $^7F_0 \rightarrow {}^5L_6$ transition (25445 cm^{-1} for [Y(TLA):Eu^{3+} (5.0 mol%)]) exhibits the highest intensity among the intraconfigurational transitions in the excitation spectra.

The emission spectra of the [RE(TLA):Eu^{3+} (x mol%)] complexes (RE^{3+}: Y, Gd and Lu), were recorded under excitation in the TLA ligand band (ca. 295 nm) at 77 K, to reduce the vibronic coupling compared to the room temperature case. The emission energy levels of $^5D_0 \rightarrow {}^7F_J$ transitions (J = 0-4) of the Eu^{3+} ion, can be attributed as the following (in cm^{-1}): $^7F_0$ (17270); $^7F_1$ (16920); $^7F_2$, (16210); $^7F_3$ (15337) and $^7F_4$ (14350), based at the [Y(TLA):Eu^{3+} 5.0 mol%)]. The efficient energy transference TLA $\rightarrow Eu^{3+}$ ion is evidenced by the absence of ligand broad emission band in the emission spectra in the spectral range from the 400 to 700 nm.

Using the optical data obtained from the emission spectra, it is possible to calculate the radiative rates ($A_{0\rightarrow J}$) from the $^5D_0 \rightarrow {}^7F_J$ transitions using equation 1:[16,17]

$$A_{0\rightarrow J} = \left(\frac{\sigma_{0\rightarrow 1}}{S_{0\rightarrow 1}}\right)\left(\frac{S_{0\rightarrow J}}{\sigma_{0\rightarrow J}}\right)A_{0\rightarrow 1} \quad (1)$$

where $\sigma_{0\rightarrow 1}$ and $\sigma_{0\rightarrow 2,4}$ correspond to the energy barycenter of the $^5D_0 \rightarrow {}^7F_1$ and $^5D_0 \rightarrow {}^7F_{2,4}$ transitions, respectively. The $S_{0\rightarrow 1}$ and $S_{0\rightarrow J}$ are the areas calculated under the emission of the spectral curve corresponding to the $^5D_0 \rightarrow {}^7F_1$ and $^5D_0 \rightarrow {}^7F_J$ transitions, respectively.[35] Since the magnetic dipole $^5D_0 \rightarrow {}^7F_1$ transition is almost insensitive to changes with the chemical environment around the Eu^{3+} ion, the $A_{0\rightarrow 1}$ rate can be used as an internal standard to determine the $A_{0\rightarrow J}$ coefficients for Eu^{3+} containing compounds.[16]

The lifetime (τ) of the luminescent compounds were obtained from the luminescence decay curve using a first order exponential decay, with excitation at the $^7F_0 \rightarrow {}^5L_6$ band. The emission quantum efficiency (η, or intrinsic

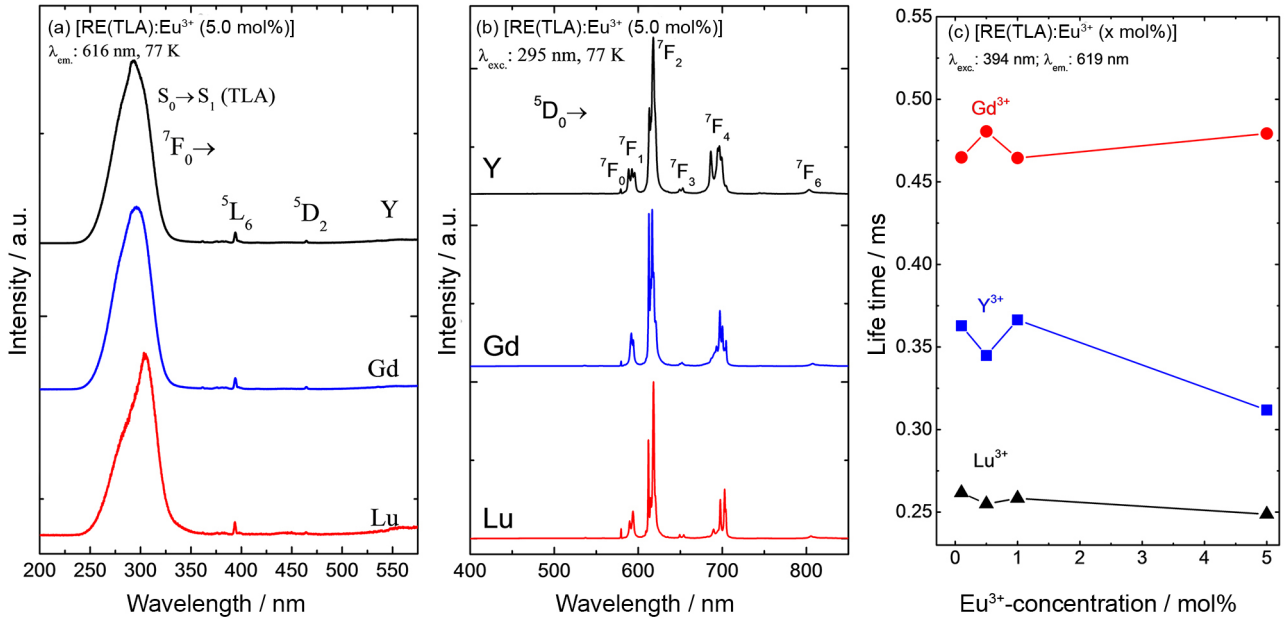

Figure 6. The (a) excitation spectra of [RE(TLA):Eu^{3+} (5.0 mol%)] (RE^{3+}: Y, Gd and Lu), with emission monitored at 616 nm; (b) emission spectra, with excitation at 295 nm, recorded at 77 K and (c) correlation between [RE(TLA):Eu^{3+} (x%)] lifetimes and Eu^{3+}-doping concentrations (x: 0.1, 0.5, 1.0 and 5.0 mol%).

quantum yield, Q_{Ln}^{Ln}, as it has been defined by Bünzli)[36] of the $^5D_0$ emitting level is determined according to equation 2:

$$\eta = \frac{A_{rad}}{A_{rad} + A_{nrad}} \quad (2)$$

where the total decay rate, $A_{tot} = 1/\tau = A_{rad} + A_{nrad}$ and the $A_{rad} = \Sigma_J A_{0\rightarrow J}$. The A_{rad} and A_{nrad} quantities are the radiative and non-radiative rates, respectively. Table 1 shows the experimental values of the radiative (A_{rad}), non-radiative (A_{nrad}) rates and $^5D_0$ emitting level emission quantum efficiency (η).

The [RE(TLA):Eu^{3+} (x mol%)] lifetime values (Table 1 and Figure 6c) show higher values for Gd^{3+} and Y^{3+} containing complexes when compared to the Lu^{3+} ion case. On the other hand, there are no changes in the lifetime behavior doping with an increasing concentration from 0.1, 0.5, 1.0 and 5.0 mol%, within the same system.

The $^5D_0 \rightarrow {}^7F_2$ and $^5D_0 \rightarrow {}^7F_4$ transitions can be used to estimate the experimental intensity parameters (Ω_λ, $\lambda = 2$ and 4). The Ω_6 intensity parameter is not included in this study since the $^5D_0 \rightarrow {}^7F_6$ transition was not observed for these systems. The coefficient of spontaneous emission, A, is given by equation 3:

$$A_{0\rightarrow J} = \frac{4e^2\omega^3}{3\hbar c^3}\chi\sum_\lambda \Omega_\lambda \left\langle {}^7F_J \middle\| U^{(\lambda)} \middle\| {}^5D_0 \right\rangle^2 \quad (3)$$

where, $\chi = n(n+2)^2/9$ is the Lorentz local field correction and n is the refractive index of the medium (refractive index used: 1.5 for all [RE(TLA):Eu^{3+}] complexes and between 1.5 and 1.6 for RE_2O_3:Eu^{3+} materials). The squared reduced matrix elements $\langle {}^7F_J \| U^{(\lambda)} \| {}^5D_J \rangle^2$ are 0.0032 and 0.0023 calculated for J = 2 and 4, respectively.[35,37]

The Ω_λ parameters depend mainly on the local geometry, bonding atoms and polarizabilities in the first coordination sphere of the RE^{3+} metal ion, and are governed by both forced electric dipole (FED) and dynamic coupling (DC) mechanisms. Moura *et al.*[38] reported that the Ω_2 parameter values are very sensitive to small angular changes in the local coordination geometry (much more than the $\Omega_{4,6}$ parameters). This spectroscopic behavior is associated with the hypersensitivity of certain 4f-4f transitions, to changes in the chemical environment, that are usually ruled by the Ω_2 intensity parameter. On the other hand, the Ω_4 and Ω_6 values are most sensitive the chemical bond distances to the ligating atoms around the lanthanide ion. Indeed, as concluded by Moura *et al.*,[38] covalency in the ion-ligand bonding becomes more important with the increasing rank of the Ω_λ, supporting the idea that the Ω_4 and Ω_6 parameters are better probes then Ω_2 to quantify covalency in these compounds.

The Ω_λ (λ = 2 and 4) parameter values for the [RE(TLA):Eu^{3+} (x mol%)] compounds (x = 0.1, 0.5, 1.0 and 5.0 mol%) are presented in Table 1. The Ω_2 values (ca. 6×10^{-20} cm^2) found for these doped complexes are systematically larger than the [RE(TMA):Eu^{3+}] (RE^{3+}: Y and Lu) anhydrous complexes (ca. 2×10^{-20} cm^2) values

Table 1. Experimental values of intensity parameters (Ω_λ), radiative (A_{rad}) and non-radiative (A_{nrad}) rates, emission lifetimes and emission quantum efficiencies of the $^5D_0$ emitting level determined for the [RE(TLA):Eu^{3+} (x mol%)] (RE^{3+}: Y, Gd and Lu) phosphors based on the emission spectra recorded at 77 K

[RE(TLA):Eu^{3+} / (x mol%)]	Ω_2 / (10^{-20} cm^2)	Ω_4 / (10^{-20} cm^2)	A_{rad} / s^{-1}	A_{nrad} / s^{-1}	A_{tot} / s^{-1}	τ / ms	η / %
Y^{3+}							
0.1	6.4	1.6	264	2492	2756	0.363	10
0.5	6.2	1.7	258	2642	2900	0.345	9
1.0	6.1	1.7	257	2475	2732	0.366	9
5.0	6.1	1.7	257	2948	3205	0.312	8
Gd^{3+}							
0.1	4.7	1.7	216	1936	2151	0.465	10
0.5	4.8	1.8	219	1862	2081	0.481	11
1.0	5.1	1.7	225	1928	2153	0.464	10
5.0	4.7	1.8	217	1870	2087	0.479	10
Lu^{3+}							
0.1	5.5	1.3	234	3587	3821	0.262	6
0.5	5.4	1.4	229	3693	3922	0.255	6
1.0	5.4	1.3	229	3641	3870	0.258	6
5.0	5.4	1.3	229	3792	4021	0.249	6

Ω_λ: experimental values of intensity parameters; A_{rad}: radiative rate; A_{nrad}: non-radiative rate; A_{tot}: total decay rate; τ: lifetime; η: quantum efficiency.

[RETMA] reported by Silva *et al*.[39] reflecting the higher hypersensitive character of the $^5D_0 \rightarrow {}^7F_2$ transition.[23,40,41]

The emission quantum efficiency values of the [RE(TLA):Eu^{3+} (x mol%)] are lower for the complexes containing Y^{3+} and Gd^{3+} (η ca. 10%) and Lu^{3+} (η ca. 6%) ions, which indicate a strong non-radiative decay pathway mediated by water molecules (Table 1). It is also observed that increasing the Eu^{3+} concentration from 0.1 to 5.0 mol% produces no change in the emission quantum efficiency values, suggesting that the luminescence quenching concentration effect is not operative for these systems.

RE_2O_3:Eu^{3+} materials

The excitation spectra of RE_2O_3:Eu^{3+} annealed phosphors (RE^{3+}: Y, Gd and Lu) were recorded at 77 K in the spectral range from 200 to 590 nm, with the emission monitored at 613 nm (Figure 7 and Figure S3). They show the presence of a broad absorption band centered around (ca. 39000 cm^{-1}) assigned to the $O^{2-}(2p) \rightarrow Eu^{3+}(4f^6)$ LMCT transition. Besides, the narrow absorption bands arisen from 4f-4f transitions from the RE^{3+} ion (ca. 17000 to 34000 cm^{-1}) are observed.

The excitation spectra recorded at 300 K (Figure S4) show the presence of the overlapped $^7F_0 \rightarrow {}^5D_1$ and $^7F_1 \rightarrow {}^5D_1$ transitions (ca. 19000 cm^{-1}) allowed by magnetic-dipole mechanism (ΔJ = 0, ±1, but 0 ↔ 0 is forbidden) for both the C_2 and S_6 symmetries. This optical results are due to the thermal population of the $^7F_1$ level that are in agreement with the results previously reported for RE_2O_3:Eu^{3+}.[42,43] The absorption bands assigned to the $^7F_0 \rightarrow {}^5D_2$ transition allowed by induced electric dipole and dynamic coupling mechanisms were observed from 21500 to 21900 cm^{-1}. In addition, a weak absorption band around 24100 cm^{-1} is assigned to the forbidden $^7F_0 \rightarrow {}^5D_3$ transition (by ΔJ selection rules) as a result of the relaxation of the selection rule due to the J-mixing effects in the ^7F_J manifolds. Moreover, the other absorption bands (Figure 7) originated from 4f-4f transitions of the Eu^{3+} ion were observed such as (in nm): the $^7F_0 \rightarrow {}^5L_6$ (394), $^5G_{2-6}$ (387), $^5L_{7,8}$ (376), $^5D_4$ (363), $^5H_{J'}$, $^5F_{J'}$, $^5I_{J'}$ and $^3P_0$ (between 286 and 335).

It is worth mentioning that the excitation spectra of the Gd_2O_3:Eu^3 present the characteristic strong absorption (nm): $^8S_{7/2} \rightarrow {}^6P_{7/2}$ (313), $^8S_{7/2} \rightarrow {}^6P_{5/2}$ (307) and $^8S_{7/2} \rightarrow {}^6P_{3/2}$ (302) transitions, indicating efficient energy transfer from the Gd^{3+} to the Eu^{3+} ion upper levels.[44] The $^8S_{7/2} \rightarrow {}^6I_J$ (J = 7/2,9/2,17/2) (276) transitions overlap with the LMCT band. This high intensity absorption band indicates an efficient Gd^{3+} to Eu^{3+} energy transfer.[45]

The luminescent materials prepared by the benzenetricarboxylate method present comparable excitation features, indicating the reproducibility of the method even when using different benzenetricarboxylate (BTC) ligands.[23]

The emission spectra of the RE_2O_3:Eu^{3+} (RE^{3+}: Y, Gd and Lu) annealed at temperatures from 500 to 1000 °C were recorded at 77 K from 400 to 750 nm, under excitation in the LMCT band at 260 nm (Figure 7). All

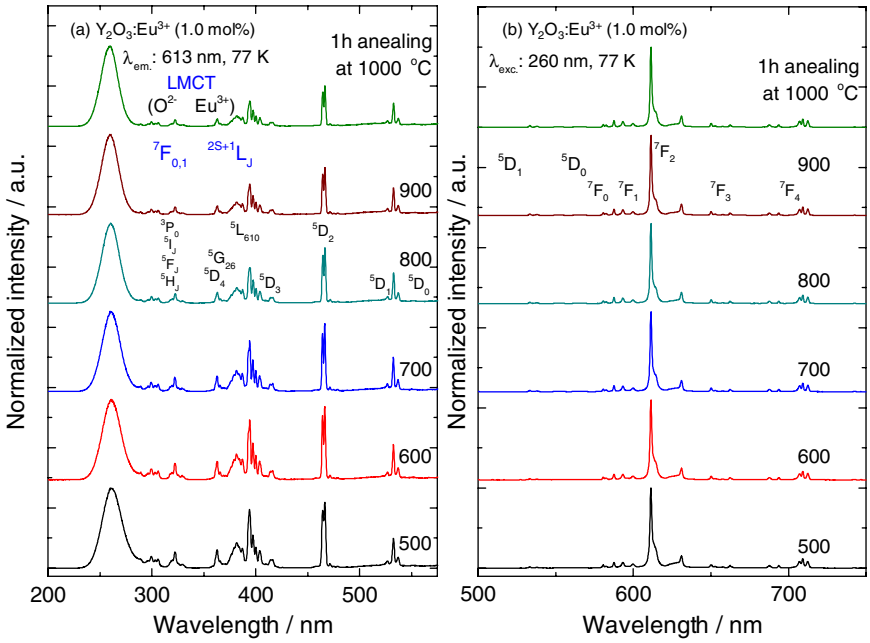

Figure 7. The (a) excitation spectra of Y_2O_3:Eu^{3+} (1.0 mol%), with emission monitored at 613 nm; (b) emission spectra, with excitation at 260 nm, recorded at 77 K.

the spectra exhibit only the sharp lines arising from the $^5D_{0,1,2,3} \rightarrow {}^7F_{0\text{-}6}$, transitions of the Eu^{3+} ion. All materials show only one emission line assigned to $^5D_0 \rightarrow {}^7F_0$ transition (ca. 17270 cm^{-1}) of the C_2 site of the cubic C-type. The $^5D_0 \rightarrow {}^7F_1$ transition is present in both sites in the region of 16666, 16846 and 17015 cm^{-1} as well at 16770 and 17165 cm^{-1} originating from the C_2 and S_6 sites.[42,43]

As reported by Boyer *et al.*[46] and Meltzer *et al.*,[47] the refractive index (n) of the bulk RE_2O_3:Eu^{3+} is around 1.9 and the $^5D_0$ lifetime (τ) of europium ion is 1.0 ms. On the other hand, these values can be different in the case of the RE_2O_3 nanostructured materials, with average sizes around 20-30 nm (crystallite size inferior to the wavelength of exciting radiation). Moreover, the morphology and surface/volume ratio of the nanoparticles may play a role in the profile of the decay curves.

The radiative rate (A_{01}) of the $^5D_0 \rightarrow {}^7F_1$ transition of Eu^{3+} ion (allowed by the magnetic dipole mechanism) is formally insensitive to the ligand field environment. Therefore it can be used as a reference transition whose value is 50 s^{-1} assuming a refractive index equal to 1.6.[17,48,49] Based on this value, the refractive indices were determined and compared to the lifetime and crystallite size values reported previously.[46-48] The experimental intensity parameters ($\Omega_{2,4}$) and lifetimes (0.8-1.9 ms) values were obtained using the effective refractive index values between 1.5 and 1.6. The values of the experimental intensity parameters ($\Omega_{2,4}$) the radiative (A_{rad}) and non-radiative (A_{nrad}) rates and emission quantum efficiencies (η) of the $^5D_0$ emitting level of the RE_2O_3:Eu^{3+} are presented in Table 2.

The values for Ω_2 (ca. 12) and Ω_4 (ca. 2-3) are very similar in the same matrix (Table 2) for different annealing temperatures as shown in the spectral profiles (Figure 7b).[50] These results are a reflection of the observed emission intensity variations of the $^5D_0 \rightarrow {}^7F_2$ transition of the Eu^{3+} ion. This optical behavior demonstrates that the Eu^{3+} ion acts as efficient luminescence probe even for the samples annealed at different temperatures. In addition, Ω_2 and Ω_4 values are also comparable changing the RE^{3+} matrix, due to the similarity in the radii in the lanthanide series.

The experimental intensity parameter values for the phosphors using the TLA ligand as precursor are smaller for all the systems, as compared to those originated from the TMA ligand, especially for the of Gd^{3+} matrix.[19]

According to Table 2, the RE_2O_3:Eu^{3+} phosphors present an emission quantum efficiency values varying from 37 to 82% with the annealing temperature of 500-1000 °C. Among the materials, the Lu_2O_3:Eu^{3+}(1.0 mol%) with annealing at 900 °C present the highest emission quantum efficiency (η = 82%). This phenomenon is probably associated to the removal of oxycarbonate from the matrices with increasing the annealing temperature. It is important to mention that the RE_2O_3:Eu^{3+} phosphors prepared by the benzenetricarboxylate method using the TLA ligand is cheaper than compared with the TMA ligand.

The Commission Internationale de l'Eclairage (CIE) chromaticity coordinates generated from the emission spectra of Eu^{3+} doped RE_2O_3 (Figure 8) are x: 0.650 and y: 0.335.[49] The color coordinates show virtually no

change for different sesquioxide matrices, concentration or annealing temperature. The phosphors containing Gd^{3+}, Y^{3+}, Lu^{3+} ions exhibit the same characteristic nearly monochromatic emission. The images of the Y_2O_3:Eu^{3+} (1.0 mol%) nanomaterials under UV irradiation show identical strong red emission for all the phosphors annealed at temperatures from 500 to 1000 °C.

Table 2. Experimental values of intensity parameters (Ω_λ), radiative (A_{rad}) and non-radiative (A_{nrad}) rates, emission lifetimes and emission quantum efficiencies of the $^5D_0$ emitting level determined for the RE_2O_3:Eu^{3+} (1.0 mol%) (RE^{3+}: Y, Gd and Lu) phosphors, annealed for 1 hour, based on the emission spectra recorded at 77 K

RE_2O_3:Eu^{3+} (1.0 mol%) / °C	Ω_2 / (10^{-20} cm^2)	Ω_4 / (10^{-20} cm^2)	A_{rad} / s^{-1}	A_{nrad} / s^{-1}	A_{tot} / s^{-1}	τ / ms	η / %
Y_2O_3:Eu^{3+}							
500	12.8	2.4	470	264	734	1.362	64
600	12.6	2.3	461	207	668	1.496	69
700	12.6	2.3	462	181	643	1.555	72
800	12.5	2.2	459	113	571	1.751	80
900	12.1	2.2	446	107	553	1.808	81
1000	11.8	2.1	435	111	546	1.830	80
Gd_2O_3:Eu^{3+}							
500	12.6	1.9	458	788	1246	0.803	37
600	12.3	1.9	447	632	1079	0.927	41
700	12.0	1.8	438	428	866	1.155	51
800	12.0	1.8	438	265	702	1.424	62
900	11.7	1.8	430	195	625	1.600	69
1000	11.4	1.7	419	166	585	1.709	72
Lu_2O_3:Eu^{3+}							
500	11.5	2.8	434	284	719	1.391	60
600	11.5	2.7	435	253	688	1.454	63
700	11.4	2.7	431	155	588	1.701	73
800	11.5	2.6	433	107	541	1.850	80
900	11.6	2.6	434	95	529	1.890	82
1000	11.2	2.5	422	104	526	1.900	80

Ω_λ: experimental values of intensity parameters; A_{rad}: radiative rate; A_{nrad}: non-radiative rate; A_{tot}: total decay rate; τ: lifetime; η: quantum efficiency.

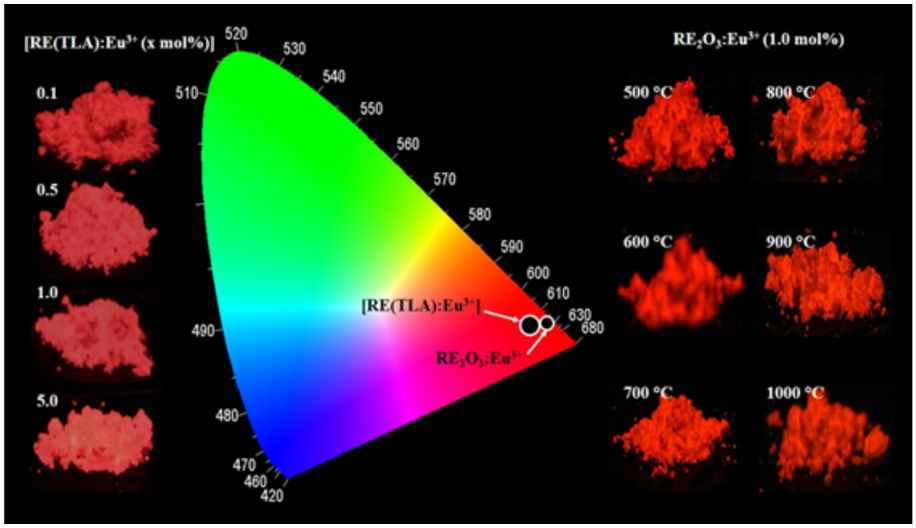

Figure 8. CIE diagram (center) and images and of [RE(TLA):Eu^{3+}] (left) and RE_2O_3:Eu^{3+} (right), excitated at 254 nm.

Conclusions

[RE(TLA):Eu^{3+}] complexes present low total decomposition temperature of the organic moistly producing the high luminescent $RE_2O_3:Eu^{3+}$ materials at 500 °C. The benzenetricarboxylate method is reliable, efficient and reproducible for the synthesis of phosphors at low temperature. The red emission of the $RE_2O_3:Eu^{3+}$ materials (RE^{3+}: Y^{3+}, Gd^{3+} and Lu^{3+}) arise mainly from the C_2 symmetry site. The large values of the Ω_2 experimental parameters corroborates with the high intensity of the $^5D_0 \rightarrow {}^7F_2$ transition. Besides, these materials can act as efficient red light conversion devices in the studied Eu^{3+}-concentration range. Finally, the $RE_2O_3:Eu^{3+}$ phosphors prepared by the benzenetricarboxylate method using the [RE(TLA):Eu^{3+}] present lower emission quantum efficiency (η close to 80%) than from the [RE(TMA):Eu^{3+}] precursor complexes (η close to 90%). However they are cheaper, becoming an efficient and more economically viable system potentially usable as optical markers.

Supplementary Information

Supplementary information is available free of charge at http://jbcs.sbq.org.br as PDF file.

Acknowledgements

The authors acknowledge financial support from Conselho Nacional de Desenvolvimento Científico e Tecnológico (CNPq), Coordenação de Aperfeiçoamento de Pessoal de Nível Superior (CAPES) and Fundação de Amparo à Pesquisa do Estado de São Paulo (FAPESP).

References

1. Mustafa, D.; Silva, I. G. N.; Bajpe, S. R.; Martens, J. A.; Kirschhock, C. E. A.; Breynaert, E.; Brito, H. F.; *Dalton Trans.* **2014**, *43*, 13480.
2. Jiblaoui, A.; Leroy-Lhez, S.; Ouk, T.-S.; Grenier, K.; Sol, V.; *Bioorg. Med. Chem. Lett.* **2015**, *25*, 355.
3. Choi, J. R.; Tachikawa, T.; Fujitsuka, M.; Majima, T.; *Langmuir* **2010**, *26*, 10437.
4. Pan, Z.-R.; Xu, J.; Yao, X.-Q.; Li, Y.-Z.; Guo, Z.-J.; Zheng, H.-G.; *CrystEngComm* **2011**, *13*, 1617.
5. Atwood, D. A.; *The Rare Earth Elements: Fundamentals and Applications*; EIC Books; Wiley: Lexington, 2013.
6. Avichezer, D.; Schechter, B.; Arnon, R.; *React. Funct. Polym.* **1998**, *36*, 59.
7. Galvão, S. B.; Lima, A. C.; de Medeiros, S. N.; Soares, J. M.; Paskocimas, C. A.; *Mater. Lett.* **2014**, *115*, 38.
8. Sugimoto, S.; *J. Phys. D: Appl. Phys.* **2011**, *44*, 064001.
9. Ma, H.; Okuda, J.; *Macromolecules* **2005**, *38*, 2665.
10. Hong, Z. R.; Liang, C. J.; Li, R. G.; Li, W. L.; Zhao, D.; Fan, D.; Wang, D. Y.; Chu, B.; Zang, F. X.; Hong, L. S.; Lee, S. T.; *Adv. Mater.* **2001**, *13*, 1241.
11. Trojan-Piegza, J.; Niittykoski, J.; Hölsä, J.; Zych, E.; *Chem. Mater.* **2008**, *20*, 2252.
12. Gawryszewska, P.; Sokolnicki, J.; Legendziewicz, J.; *Coord. Chem. Rev.* **2005**, *249*, 2489.
13. Cotton, S.; *Spectrochim. Acta, Part A* **1990**, *46*, 1797.
14. Kumar, P.; Dwivedi, J.; Gupta, B. K.; *J. Mater. Chem. C* **2014**, *2*, 10468.
15. Moine, B.; Bizarri, G.; *Opt. Mater.* **2006**, *28*, 58.
16. Brito, H. F.; Malta, O. L.; Felinto, M. C. F. C.; Teotonio, E. E. S. In *The Chemistry of Metal Enolates, Part 1*; John Wiley & Sons: West Sussex, England, 2009.
17. De Sá, G. F.; Malta, O. L.; Donegá, C. M.; Simas, A. M.; Longo, R. L.; Santa-Cruz, P. A.; da Silva, E. F.; *Coord. Chem. Rev.* **2000**, *196*, 165.
18. Biggemann, D.; Mustafa, D.; Tessler, L. R.; *Opt. Mater.* **2006**, *28*, 842.
19. Souza, E. R.; Silva, I. G. N.; Teotonio, E. E. S.; Felinto, M. C. F. C.; Brito, H. F.; *J. Lumin.* **2010**, *130*, 283.
20. Kodaira, C. A.; Brito, H. F.; Felinto, M. C. F. C.; *J. Solid State Chem.* **2003**, *171*, 401.
21. Huang, H.; Xu, G. Q.; Chin, W. S.; Gan, L. M.; Chew, C. H.; *Nanotechnology* **2002**, *13*, 318.
22. Aitasalo, T.; Dereń, P.; Hölsä, J.; Jungner, H.; Lastusaari, M.; Niittykoski, J.; Stręk, W.; *Radiat. Meas.* **2004**, *38*, 515.
23. Silva, I. G. N.; Rodrigues, L. C. V.; Souza, E. R.; Kai, J.; Felinto, M. C. F. C.; Hölsä, J.; Brito, H. F.; Malta, O. L.; *Opt. Mater.* **2015**, *40*, 41.
24. Nakamoto, K.; *Infrared and Raman Spectra of Inorganic and Coordination Compounds*; John Wiley & Sons: New York, 1997.
25. Silva, I. G. N.; Kai, J.; Felinto, M. C. F. C.; Brito, H. F.; *Opt. Mater.* **2013**, *35*, 978.
26. Łyszczek, R.; *J. Therm. Anal. Calorim.* **2007**, *90*, 533.
27. Shannon, R. D.; *Acta Crystallogr.* **1976**, *32*, 751.
28. Vegard, L.; *Z. Phys.* **1921**, *5*, 17.
29. Hölsä, J.; Turkki, T.; *Thermochim. Acta* **1991**, *190*, 335.
30. Davolos, M. R.; Feliciano, S.; Pires, A. M.; Marques, R. F. C.; Jafelicci, M.; *J. Solid State Chem.* **2003**, *171*, 268.
31. Klug, H. P.; Alexander, L. E.; *X-ray Diffraction Procedures for Polycrystalline and Amorphous Materials*; Wiley: New York, 1975.
32. Adachi, G.; Imanaka, N.; *Chem. Rev.* **1998**, 1479.
33. Ren, H.; Liu, G.; Song, X.; Hong, G.; Cui, Z.; *Proc. SPIE 6029, ICO20: Materials and Nanostructures* **2006**, 60291S.
34. Wang, F.; Deng, K.; Wu, G.; Liao, H.; Liao, H.; Zhang, L.; Lan, S.; Zhang, J.; Song, X.; Wen, L.; *J. Inorg. Organomet. Polym. Mater.* **2012**, *22*, 680.

35. Teotonio, E. E. S.; Fett, G. M.; Brito, H. F.; Faustino, W. M.; de Sá, G. F.; Felinto, M. C. F. C.; Santos, R. H. A.; *J. Lumin.* **2008**, *128*, 190.
36. Bünzli, J. C. G.; *Coord. Chem. Rev.* **2015**, *293*, 19.
37. Carlos, L. D.; Messaddeq, Y.; Brito, H. F.; Ferreira, R. A. S.; Bermudez, V. Z.; Ribeiro, S. J. L.; *Adv. Mater.* **2000**, *12*, 594.
38. Moura, R. T.; Carneiro Neto, A. N.; Longo, R. L.; Malta, O. L.; *J. Lumin.* **2015**, *in press*, DOI: 10.1016/j.jlumin.2015.08.016.
39. Silva, I. G. N.; Mustafa, D.; Andreoli, B.; Felinto, M. C. F. C.; Malta, O. L.; Brito, H. F.; *J. Lumin.* **2015**, *in press*, DOI: 10.1016/j.jlumin.2015.04.047.
40. Ferreira, R. A. S.; Nobre, S. S.; Granadeiro, C. M.; Nogueira, H. I. S.; Carlos, L. D.; Malta, O. L.; *J. Lumin.* **2006**, *121*, 561.
41. Silva, I. G. N.; Brito, H. F.; Souza, E. R.; Mustafa, D.; Felinto, M. C. F. C.; Carlos, L. D.; Malta, O. L.; *Z. Z. Naturforsch., B: J. Chem. Sci.* **2013**, *69b*, 231.
42. Zych, E.; Karbowiak, M.; Domagala, K.; Hubert, S.; *J. Alloys Compd.* **2002**, *341*, 381.
43. Karbowiak, M.; Zych, E.; Holsa, J.; *J. Phys.: Condens. Matter* **2003**, *15*, 2169.
44. Buijs, M.; Meyerink, A.; Blasse, G.; *J. Lumin.* **1987**, *37*, 9.
45. Macedo, A. G.; Ferreira, R. A. S.; Ananias, D.; Reis, M. S.; Amaral, V. S.; Carlos, L. D.; Rocha, J.; *Adv. Funct. Mater.* **2010**, *20*, 624.
46. Boyer, J. C.; Vetrone, F.; Capobianco, J. A.; Speghini, A.; Bettinelli, M.; *J. Phys. Chem. B* **2004**, *108*, 20137.
47. Meltzer, R. S.; Feofilov, S. P.; Tissue, B.; Yuan, H. B.; *Phys. Rev. B* **1999**, *60*, R14012.
48. Whiffen, R. M. K.; Antić, Ž.; Speghini, A.; Brik, M. G.; Bártová, B.; Bettinelli, M.; Dramićanin, M. D.; *Opt. Mater.* **2014**, *36*, 1083.
49. Santa-Cruz, P. A.; Teles, F. S.; *Spectra Lux Software v.2.0 Beta*, Ponto Quântico Nanodispositivos, RENAMI, **2003**.
50. Binnemans, K.; *Coord. Chem. Rev.* **2015**, *295*, 1.

Submitted: August 26, 2015
Published online: November 16, 2015

FAPESP has sponsored the publication of this article.